Applied Surface Science 45 (1990) 37–48
North-Holland

Angle-resolved X-ray photoelectron spectroscopy (ARXPS) and a modified Levenberg–Marquardt fit procedure: a new combination for modeling thin layers

W.A.M. Aarnink, A. Weishaupt and A. van Silfhout
University of Twente, Faculty of Applied Physics, P.O. Box 217, N-7500 AE Enschede, The Netherlands

Received 14 November 1989; accepted for publication 16 March 1990

The combination of angle-resolved X-ray photoelectron spectroscopy (ARXPS) and a modified Levenberg–Marquardt (LM) fit procedure has been used to study a native oxide layer on a clean Si(100) substrate. Numerical calculations show that with an aperture of 3° or 9° of the electron analyser, the photoelectron take-off angle should not exceed 80° or 70°, respectively, as compared to normal take-off angles. At larger photoelectron take-off angles, the effect of the aperture on the photoelectron energy distribution may not be neglected. We show how absolute ARXPS measurements in which the same XPS feature is considered at several electron take-off angles are an alternative for relative ARXPS film thickness measurements, avoiding large errors in the quantitative results. Models for the composition and thickness of the oxide layer have been developed. Also, the errors in the parameters of these models have been calculated. It can be concluded that the native oxide layer on silicon is 27 ± 1 ($\pm 5\%$) Å thick and that the ratio of the silicon atom concentration in the substrate to that in the native oxide layer is 3.7 ± 0.3 ($\pm 8\%$), values that agree well with the literature. This report shows that the combination of ARXPS and a LM fit procedure is well suited to study ultra-thin layers and gives reliable results.

1. Introduction

Angle-resolved X-ray photoelectron spectroscopy (ARXPS) is a widely used non-destructive method to study the chemical composition and thickness of the outermost toplayer of solid materials (thickness ≤ 6 nm) and therefore very attractive for the investigation of very thin layers [1–11]. The depth range of the method is limited by the effective escape depth of the photoelectrons in the toplayer of the material and within this range (≤ 6 nm) the thickness of the layer can be obtained from the ratio of the measured angular peak intensities between the film and substrate. Fadley [1–3] and others [4,5,11] have demonstrated that surface roughness significantly influences the spectral intensities of photoelectrons, particularly at higher photoelectron take-off angles.

However, as we will show in this paper, the influence of the width of the acceptance angle of the photoelectron energy analyser is even more important for the accuracy of the thickness measurements.

Usually, the peak intensity $I(\varphi)$ of an XPS peak at photoelectron take-off angle φ of element i is given by (see fig. 1):

$$I_i(\varphi) \propto T_{\text{tot}}(\varphi)\, F(\varphi)\, \sigma_i \int n_i(z) \exp\left(-\frac{z}{\lambda_i \cos \varphi}\right) \mathrm{d}z, \tag{1}$$

in which T_{tot} is the transmission of the photoelectron energy analyser, F is the X-ray flux, σ_i is the photoionization cross section of element i, n_i is the concentration of element i as a function of depth z and λ_i is the in-elastic mean free path (IMFP) of the photoelectrons [12,13].

In eq. (1), the effect of the acceptance angle (aperture) of the photoelectron energy analyzer has been neglected. To demonstrate the influence of aperture on the energy distribution of the photoelectrons in section 2 of this paper an expression for this energy distribution will be derived. Numerical calculations

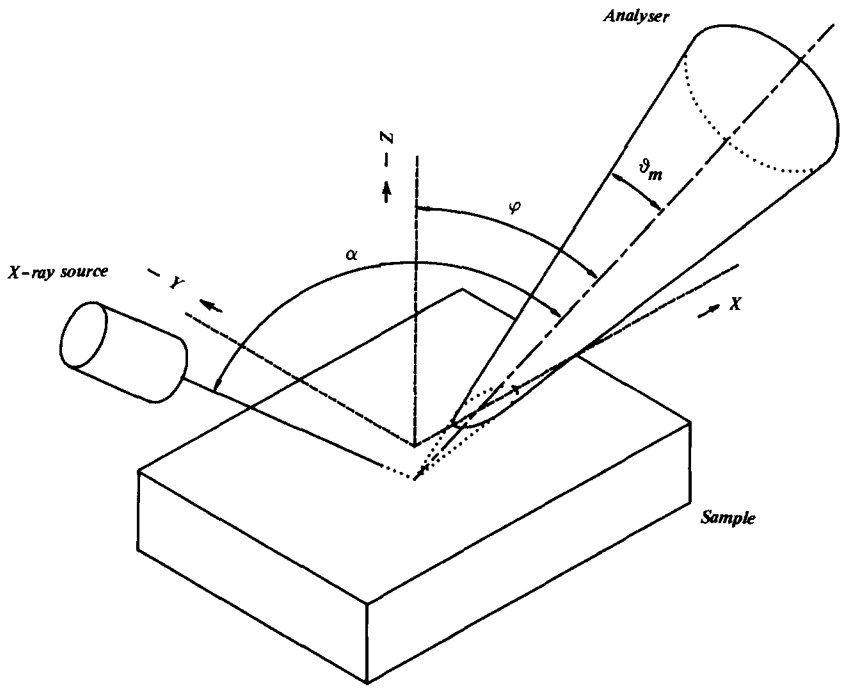

Fig. 1. Geometry of experiment set-up.

have been performed to determine the region of photoelectron take-off angles where the effect of aperture may be neglected, permitting the use of eq. (1).

By means of eq. (1), quantitative information, for example the thickness of a surface layer, can be obtained by comparing the peak intensities of the elements present in the substrate and surface layer, taken at varying photoelectron take-off angle φ [1–3,9,11]. In sections 3 and 5, we will show that these ARXPS ratio measurements (or: relative ARXPS measurements) may induce large errors in determining film thicknesses. The commonly used method, relative ARXPS measurements, contains two parameters: the film thickness and a constant containing the ratios of atomic concentrations and inelastic mean free paths of the photoelectrons in the substrate and the film. Due to a strong correlation between these two parameters, large errors in the calculated film thickness may be expected.

Therefore, in section 3 we propose an alternative way of obtaining quantitative information, by looking at the same XPS peak at varying photoelectron take-off angle and normalizing its intensity to the normal take-off angle. This method we call absolute ARXPS measurements. In this method, we have to determine the angle-dependent terms in eq. (1) quantitatively. In section 3, we will show how the effects of changing X-ray flux and photoelectron energy analyser transmission can be included in our calculations and how these absolute ARXPS measurements are analysed. With this method, we are able to eliminate one parameter and, because now only one parameter – the film thickness – is used to describe these absolute ARXPS measurements, this parameter can be calculated with much higher accuracy. In combination with our data analysis by means of a modified Levenberg–Marquardt method, as described in section 3, these absolute ARXPS measurements enable us to obtain reliable quantitative information.

To illustrate the possibilities in this way of interpreting ARXPS measurements, we studied a native oxide layer on top of a silicon substrate. The experimental set-up and data acquisition are described in section 4. Results are given in section 5. A modified Levenberg–Marquardt fit procedure is used to optimize the model of the native oxide layer, giving the thickness of the layer and the atomic concentration

ratio of the silicon in substrate and layer. Also errors in these parameters have been calculated. These calculations show that absolute ARXPS measurements can reduce the error in determining a film thickness with a factor of two, when compared with relative ARXPS film thickness measurements.

As discussed in section 6, the combination of absolute and relative ARXPS measurements and a modified Levenberg–Marquardt fit procedure is a strong and reliable method in analyzing thin films and obtaining quantitative information.

2. Effect of photoelectron energy analyser acceptance angle (aperture)

The photoelectron energy distribution $\mathrm{d}I_{i,k}(E)$ from orbital k in element i, detected at photoelectron take-off angle φ may be written as (see figs. 1 and 2) [1–3]:

$$\mathrm{d}I_{i,k} = \eta \int_x \int_y \int_z T_{\mathrm{tot}} F n_i \left(\int_0^{2\pi} \int_0^{\vartheta_m} \gamma_{i,k}\, \mathrm{e}^{-s/\lambda_i} \sin\vartheta\, \mathrm{d}\vartheta\, \mathrm{d}\phi \right) \mathrm{d}x\, \mathrm{d}y\, \mathrm{d}z\, \mathrm{d}E, \tag{2}$$

where ϑ_m denotes the photoelectron analyser acceptance angle (aperture). The electron detector has an efficiency $\eta(E_d)$ with E_d the kinetic energy of the photoelectrons after being transmitted through the lense and just before entering the electron detector. $T_{\mathrm{tot}}(\vartheta, \phi, E, E_d)$ is the total transmission of the analyser. The X-ray flux inside the sample is given by $F(x, y, \varphi)$ and $n_i(x, y, z)$ is the concentration of element i. The probability of an electron absorbing an X-ray dose and being ejected from orbital k in element i with an energy $(E, \mathrm{d}E)$ is given by $\gamma_{i,k}(\vartheta_k, E)$, the angular differential photoionization cross-section, where ϑ_k is the angle between photon and photoelectron path. $s(z, \varphi, \vartheta, \phi)$ denotes the distance the electron has to travel through the solid before it reaches the surface and $\lambda_i(E)$ is the inelastic mean free path of the photoelectrons inside the material.

Because of the high kinetic energy (500–1500 eV), interactions between photoelectrons and the surface of the sample are neglected [14]. With a small aperture ϑ_m of the analyser, elastic scattering of photoelectrons during transport through the solid can be neglected [15]. The energy distribution $\mathrm{d}I_{i,k}$ strongly depends on the total transmission T_{tot} of the analyser. In a first approximation this transmission can be described by a cone-shaped function. Within the cone the total transmission only depends on the kinetic energy E of the photoelectrons. Outside the cone the transmission equals zero (see fig. 1). Because the penetration depth of X-ray quanta is much larger than the escape depth of the photoelectrons, the flux F may be taken as being independent of depth z. In our experimental set-up, described in section 4, diffraction of X-rays at the sample surface can be neglected [16]. The angular differential cross-section $\gamma_{i,k}(\vartheta_k, E)$ may be written as:

$$\gamma_{i,k}(\vartheta_k, E) = \frac{\mathrm{d}\sigma_{i,k}(E)}{\mathrm{d}E} \frac{1}{4\pi} \left[1 - \tfrac{1}{4}\beta_{i,k}\left(3\cos^2\vartheta_k - 1\right) \right], \tag{3}$$

where $\mathrm{d}\sigma_{i,k}$ is the differential cross section [17] and $\beta_{i,k}$ the asymmetric factor [18,19]. It is assumed that eq. (3) is valid in the case of amorphous materials or if the sample consists of randomly oriented crystallites. For ϑ_k, the angle between photon and photoelectron path, we may write (see fig. 2):

$$\cos\vartheta_k = -\sin\alpha \sin\vartheta \cos\phi + \cos\alpha \cos\vartheta. \tag{4}$$

Numerical calculations showed that, with a small aperture ($\vartheta_m < 10°$), eq. (4) may be rewritten:

$$\cos\vartheta_k = \cos\alpha. \tag{5}$$

The distance the photoelectron has to travel through the solid along the direction (ϑ, ϕ) before it reaches the surface, is given by (see figs. 1 and 2):

$$s(z, \varphi, \vartheta, \phi) = z/(\cos\varphi \cos\vartheta + \sin\varphi \sin\vartheta \cos\phi). \tag{6}$$

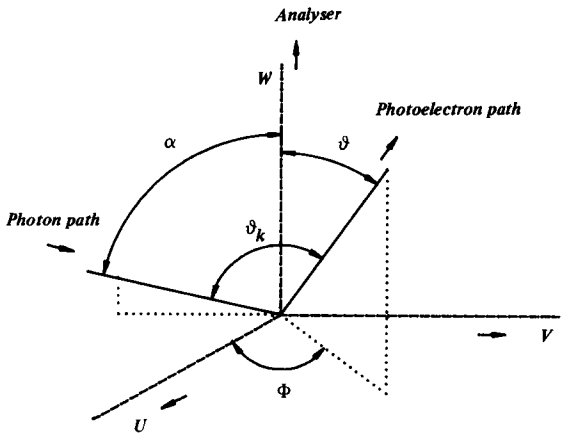

Fig. 2. Definition of angles used to calculate the angular differential cross-section $\gamma(\vartheta_k, E)$ and path $s(\varphi, \vartheta, \phi)$, which the photoelectron has to travel before reaching the sample surface. The w-axis is directed along the centre of the detection cone in fig. 1. The u-axis is the rotation axis of the sample.

Considering all this, we may rewrite eq. (2) and the photoelectron energy distribution $\mathrm{d}I_{i,k}$ is given by:

$$\mathrm{d}I_{i,k} = \eta\gamma_{i,k}\int_x\int_y T_{\mathrm{tot}} F \,\mathrm{d}x\,\mathrm{d}y \times \int_z n_i \left[\int_0^{2\pi}\int_0^{\vartheta_m} \exp\left(\frac{-z}{\lambda_i(\cos\varphi\cos\vartheta + \sin\varphi\sin\vartheta\cos\phi)}\right)\sin\vartheta\,\mathrm{d}\vartheta\,\mathrm{d}\phi\right]\mathrm{d}z\,\mathrm{d}E, \tag{7}$$

where the concentration n_i only depends on depth.

To determine the aperture at which its effect on the photoelectron energy distribution may be neglected, we define an effective depth coordinate z_{eff} and write:

$$\mathrm{d}I_{i,k} = \eta\gamma_{i,k}\int_x\int_y T_{\mathrm{tot}} F \,\mathrm{d}x\,\mathrm{d}y\, 2\pi(1-\cos\vartheta_m)\int_z n_i \exp\left(-\frac{z_{\mathrm{eff}}}{\lambda_i\cos\varphi}\right)\mathrm{d}z\,\mathrm{d}E. \tag{8}$$

Now we can define a function $f(\vartheta_m, \varphi)$ as follows:

$$z_{\mathrm{eff}} = z\left[1 + f(\vartheta_m, \varphi)\right], \tag{9}$$

and we may write:

$$\exp\left(\frac{-z\left[1+f(\vartheta_m,\varphi)\right]}{\lambda_i\cos\varphi}\right) = \frac{1}{2\pi(1-\cos\vartheta_m)}\int_0^{2\pi}\int_0^{\vartheta_m}\exp\left(\frac{-z}{\lambda_i(\cos\varphi\cos\vartheta+\sin\varphi\sin\vartheta\cos\phi)}\right)\sin\vartheta\,\mathrm{d}\vartheta\,\mathrm{d}\phi. \tag{10}$$

From this equation we can numerically calculate the function $f(\vartheta_m, \varphi)$, which provides us the boundaries of ϑ_m and φ at which the influence of the aperture on the photoelectron energy distribution may be neglected. Therefore, we integrated eq. (10) numerically for different values of depth z and photoelectron take-off angle φ. The results are given in figs. 3 and 4, where the aperture ϑ_m equals 3° and 9°, respectively. The function f is plotted as a function of depth z in λ for different photoelectron take-off angles φ. The dotted line connects the values of the function f at the information depth, which equals $3\lambda\cos\varphi$, for different values of the take-off angle φ. If we demand:

$$|f(\vartheta_m, \varphi)| < 0.1, \qquad 0 \le z \le 3\lambda\cos\varphi, \tag{11}$$

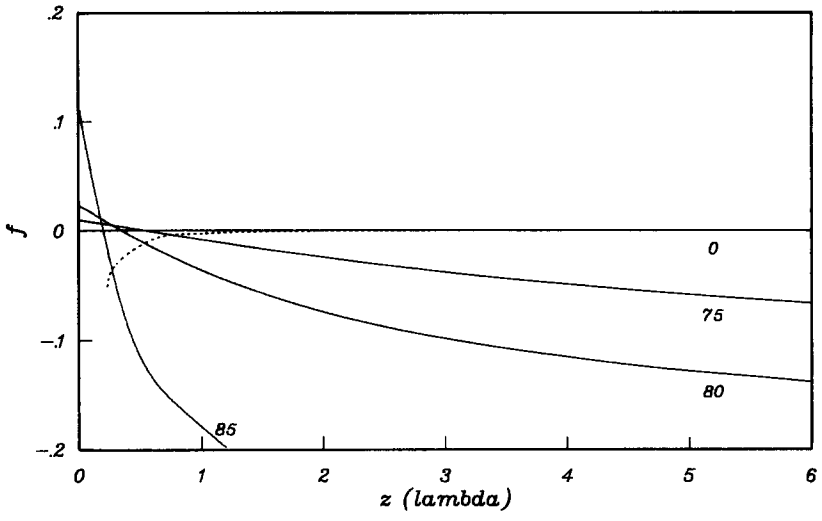

Fig. 3. Function $f = f(\vartheta_m, \varphi)$ as a function of depth z (in λ), calculated with $\vartheta_m = 3°$. The dotted line represents f at the information depth, which equals $3\lambda \cos \varphi$. For a description, see section 2.

then the influence of the aperture on the photoelectron energy distribution may be neglected at the conditions:

$$\vartheta_m = 3°, \quad 0° \leq \varphi \leq 80° \qquad \text{and} \qquad \vartheta_m = 9°, \quad 0° \leq \varphi \leq 70°, \tag{12}$$

and the photoelectron energy distribution may be written as:

$$\mathrm{d}I_{i,k} = \eta \gamma_{i,k} \int_x \int_y T_{\mathrm{tot}} F \,\mathrm{d}x \,\mathrm{d}y \, 2\pi(1 - \cos \vartheta_m) \int_z n_i \exp\left(- \frac{z}{\lambda_i \cos \varphi} \right) \mathrm{d}z \,\mathrm{d}E. \tag{13}$$

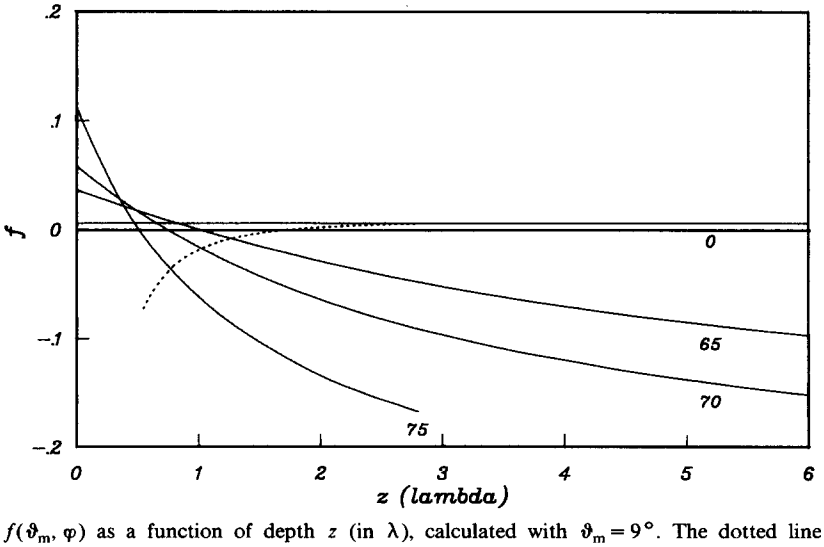

Fig. 4. Function $f = f(\vartheta_m, \varphi)$ as a function of depth z (in λ), calculated with $\vartheta_m = 9°$. The dotted line represents f at the information depth, which equals $3\lambda \cos \varphi$. For a description, see section 2.

3. Relative and absolute ARXPS measurements – data analysis

The intensity $I_{i,k}$ of an XPS peak is defined as:

$$I_{i,k} = \int_E \mathrm{d}I_{i,k}(E)\,\mathrm{d}E, \tag{14}$$

with $\mathrm{d}I_{i,k}(E)$ the photoelectron energy distribution. In our experimental set-up and for the sample we investigated, eq. (13) is valid. In this section, we will discuss two ways of performing angle-resolved X-ray photoelectron spectroscopy measurements: the commonly used relative measurements and the way we propose, absolute measurements. For both, we will derive a model for a substrate covered with an oxide layer, and we will show how the parameters in these models can be optimized with a modified Levenberg–Marquardt method and how errors in these parameters can be calculated.

3.1. Relative ARXPS measurements

The ratio R of the mean number of electrons emitted by the silicon in the bulk and the silicon in the oxide layer from the 2p orbitals as a function of electron take-off angle φ is, with eqs. (13) and (14), given by [1–5,9–11]:

$$R = \frac{I_{\mathrm{Si},2p}(\varphi)}{I_{\mathrm{SiO_2},2p}(\varphi)} = \frac{n_{\mathrm{Si}}}{n_{\mathrm{SiO_2}}}\frac{\lambda_{\mathrm{Si}}}{\lambda_{\mathrm{SiO_2}}}\left[\exp\left(\frac{d}{\lambda_{\mathrm{SiO_2}}\cos\varphi}\right)-1\right]^{-1} = C\left[\exp\left(\frac{d}{\lambda_{\mathrm{SiO_2}}\cos\varphi}\right)-1\right]^{-1}, \tag{15}$$

where n_{Si} and $n_{\mathrm{SiO_2}}$ are the atomic concentrations of silicon in the substrate and native oxide layer, respectively. The oxide layer is assumed to have a uniform thickness d. The inelastic mean free paths (IMFP) of the photoelectrons in the substrate and oxide layer are denoted by λ_{Si} and $\lambda_{\mathrm{SiO_2}}$, respectively. The ratio of the intensities of the XPS peaks of the silicon in the bulk and in the oxide layer, measured at different photoelectron take-off angles φ, could enable us to find the thickness of the oxide layer and the atomic concentration ratio of the silicon in the layer and substrate. As will be shown in section 5, problems arise due to a strong correlation between two parameters: the thickness d and the constant C.

3.2. Absolute ARXPS measurements

If we look at the same XPS peak of element i at different electron take-off angles φ and normalize its intensity to the intensity at normal take-off angle, we obtain:

$$N = \frac{I_{i,k}(\varphi)}{I_{i,k}(0)} = \frac{\int_x\int_y T_{\mathrm{tot}}F(x,\,y,\,\varphi)\,\mathrm{d}x\,\mathrm{d}y}{\int_x\int_y T_{\mathrm{tot}}F(x,\,y,\,0)\,\mathrm{d}x\,\mathrm{d}y}\,\frac{\int_0^\infty n_i\exp[-z/(\lambda_i\cos\varphi)]\,\mathrm{d}z}{\int_0^\infty n_i\exp(-z/\lambda_i)\,\mathrm{d}z}. \tag{16}$$

If the 2p peak on a clean silicon sample is measured, eq. (16) results in:

$$N = \frac{I_{\mathrm{Si},2p}(\varphi)}{I_{\mathrm{Si},2p}(0)} = \frac{\int_x\int_y T_{\mathrm{tot}}F(x,\,y,\,\varphi)\,\mathrm{d}x\,\mathrm{d}y}{\int_x\int_y T_{\mathrm{tot}}F(x,\,y,\,0)\,\mathrm{d}x\,\mathrm{d}y}\cos\varphi = G(\varphi). \tag{17}$$

So this function $G(\varphi)$, depending on the geometry of the experimental set-up, sample and sample holder, can be measured directly and this value can be used in eq. (16).

For the intensity of the 2p peak of silicon below the native oxide layer, measured at different electron take-off angles and normalized to its intensity at normal take-of angle, we may write by using eqs. (16) and (17):

$$N = \frac{I_{\mathrm{Si,2p}}(\varphi)}{I_{\mathrm{Si,2p}}(0)} = G(\varphi)\exp\left[\frac{d}{\lambda_{\mathrm{SiO_2}}}\left(1 - \frac{1}{\cos\varphi}\right)\right], \tag{18}$$

which enables us to determine the thickness d of the oxide layer on top of a silicon substrate. In deriving eq. (18), we assumed that the native oxide layer has a uniform thickness d and that in the oxide layer the inelastic mean free paths of the photoelectrons are the same for all SiO_x and can be described by λ_{SiO_2}. In eq. (18), effects of surface roughness have been neglected. By using formula (18), we do not need to know the ratio of the atomic concentrations of silicon in the substrate and oxide layer. So with this method, we are able to eliminate one parameter: the constant C in eq. (15) and, therefore, the thickness d, the other parameter, can be determined more accurately. Therefore this way of interpreting XPS data is very attractive in the case of surface layers, on top of substrates or layers with unknown concentrations of the elements present in it.

3.3. Data analysis by a modified Levenberg–Marquardt (LM) method

Using eqs. (15) and (18), we modelled a native oxide layer on top of a silicon substrate in two ways, respectively describing relative and absolute ARXPS measurements. These models contain two parameters: the thickness d and a constant C, and one parameter, the thickness d, respectively. These parameters can be optimized by minimizing the error function $F_{R,N}$:

$$F_{R,N} = \sum_{\varphi_i}\left(Y_{R,N}(\varphi_i) - Y^{\mathrm{exp}}_{i,R,N}\right)^2, \tag{19}$$

where $Y_{R,N}(\varphi_i)$ is the predicted value and $Y^{\mathrm{exp}}_{i,R,N}$ is the measured value at electron take-off angle φ_i of quantity Y. The indices R and N indicate the model that is being optimized: eq. (15) and eq. (18) respectively. The minimization is performed by a modified Levenberg–Marquardt method which yields the optimized parameters [20]. Also the residue S, defined as [21]:

$$S_{R,N} = F_{R,N}/(K - 1 - p), \tag{20}$$

where K is the number of measurements and p the number of parameters in the model, has been calculated. In combination with the confidence limits, calculated using the variance–covariance matrix, this provides a good check for the quality of the fit and gives an indication of the correlation between the parameters in the model [21].

4. Experimental

The sample we used for our measurements was cut from a polished silicon (111) wafer, as-received (p-type, 2000 Ω cm). This sample with a native oxide layer was cleaned with iso-propyl alcohol before mounting and got no further treatment.

The ARXPS experiments were carried out on a Kratos XSAM 800 spectrometer, controlled by a PDP 11 microcomputer, with a base pressure of 4×10^{-10} Torr. The photoelectron energy analyser acceptance angle was fixed at 9° (low magnification) [22]. The spectrometer was calibrated by measuring the Cu $2p_{3/2}$ peak and the X-ray induced Cu L_3MM Auger peak on a clean, sputtered copper sample using a Mg anode [23], and its linearity was checked.

The spectra were taken and simulated using the DS800 program [24]. For background subtraction, we used the method of Shirley [25]. In all simulations, 100% Gaussians were used. The positions of these Gaussians were held at the same energies at all photoelectron take-off angles, only their intensities were allowed to change to obtain the best simulation.

5. Results

5.1. Relative ARXPS measurements

In fig. 5, two XPS spectra of the Si 2p peak are shown, taken at electron take-off angle φ of 3° and 63° respectively (after an correction for the offset). With increasing photoelectron take-off angles, we see a strong increase in the intensities of the features of oxidized silicon at higher binding energies, as compared to the feature at low binding energy, the silicon in the substrate.

The spectra have been simulated by five Gaussians. The first Gaussian at a binding energy of 99.4 eV has been assigned to silicon in the substrate, the fifth Gaussian at 103.2 eV to silicon dioxide in the native oxide layer (Si^{4+}). The remaining Gaussians at 100.4, 101.1 and 101.9 eV have been ascribed to partially oxidized silicon in the native oxide layer (Si^{1+}, Si^{2+} and Si^{3+}, respectively) [26,27]. To determine the peak-intensity ratio of silicon in the substrate to that in the oxide layer we calculated the ratio of the area of the first Gaussian, the peak of silicon in the substrate, and the sum of the four Gaussians at higher binding energies, that is, the total area of the peaks of oxidized silicon. In fitting eq. (15) with a modified Levenberg–Marquardt fit procedure [20] with two parameters simultaneously, we find:

$$d = 0.8 \pm 0.1\lambda_{SiO_2}\ (\pm 13\%), \quad C = 2.7 \pm 0.7\ (\pm 30\%), \quad \text{residue } S_R = 8 \times 10^{-3}.$$

The errors in thickness d and constant C have been determined by calculating the variance–covariance matrix [21]. The large errors in the parameters may be due to: (i) statistical errors in the measurements or (ii) a strong correlation between the two parameters. If only the change in the residue is small with variations in d and C, these parameters correlate. In section 5.3, a correction on these relative ARXPS measurements will be given and it will be shown that the large errors in d and C are due to strong correlation.

The results are shown in fig. 6, where the measurements are indicated with "+" and the calculated values are shown as a solid line, where thickness d and constant C equal $0.8\lambda_{SiO_2}$ and 2.7, respectively.

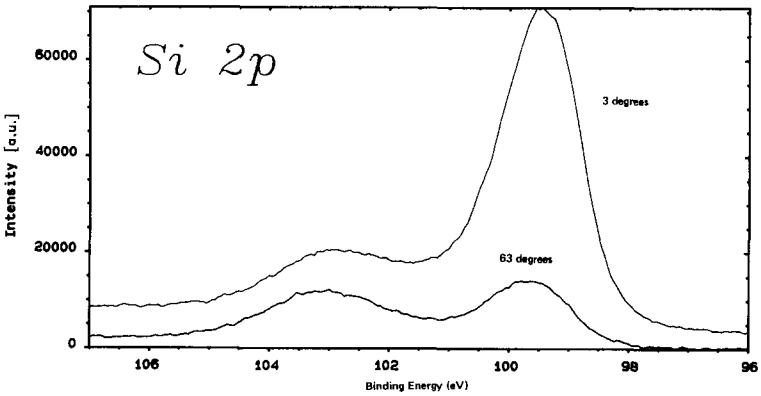

Fig. 5. Si 2p XPS peaks, taken at photoelectron take-off angles of 3° and 63°, respectively. They have been simulated with five Gaussians. For an assignment, see section 5.

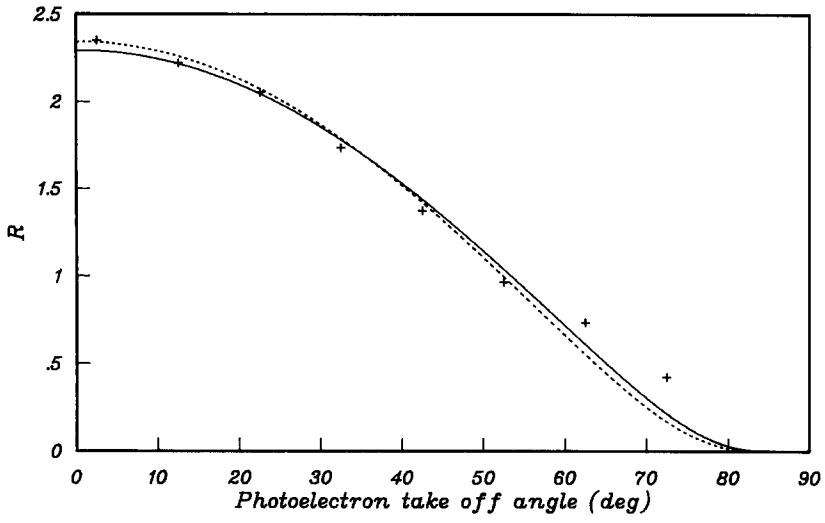

Fig. 6. Relative ARXPS measurements, the intensity ratios R of silicon in the substrate to that in the oxide layer are indicated with "+". Also the theoretical curves are shown. The solid line indicates relative ARXPS measurements, the dotted line a correction on these measurements. For a description, see sections 3.1 and 3.3.

5.2. Absolute ARXPS measurements

We measured the function $G(\varphi)$, as defined in eq. (17), in our equipment on a clean amorphous silicon substrate and the results are given in fig. 7. We performed measurements to establish the stability of the spectrometer: points marked with "+" were measured within 10 h. After 24 h, the points marked with "□" were measured, with the same instrumental settings. We see that the stability is sufficient. The solid line represents a polynomial fit of $G(\varphi)$.

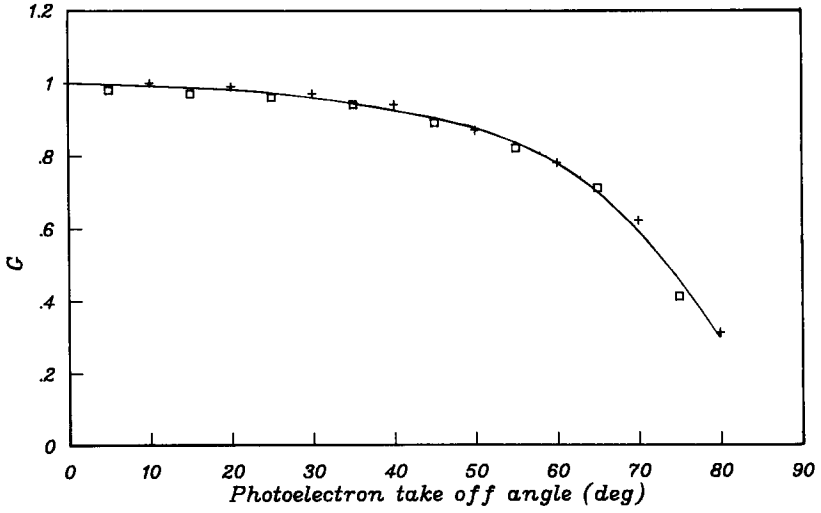

Fig. 7. Measured function $G(\varphi)$, using a clean sputtered Si sample, mounted exactly the same as the sample measured on. The solid line represents a polynomial fit. For a description, see section 3.2.

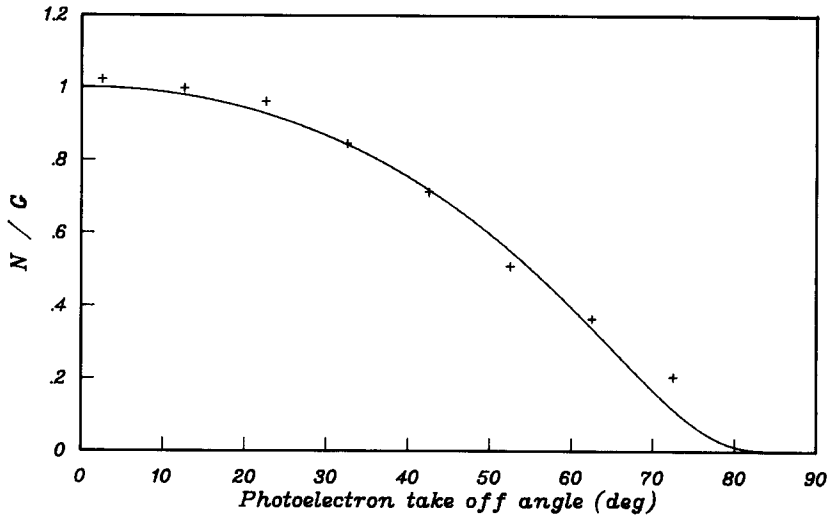

Fig. 8. Absolute ARXPS measurements, indicated with "+". The intensity of feature 1 in the Si 2p XPS spectra has been normalized to its intensity at normal take-off angle and divided by the function G, giving N/G. The theoretical curve is shown as a solid line. For a description, see section 3.2.

In fig. 8, the intensities of the first Gaussian, normalized to the intensity at normal take-off angle and divided by $G(\varphi)$, are given. When these measurements are fitted using eq. (18), containing only one parameter, we find:

$$d = 0.93 \pm 0.05\lambda_{SiO_2}\ (\pm 5\%), \quad \text{residue } S_N = 9 \times 10^{-4}.$$

The result of the fit is shown as a solid line in fig. 8. We see that the error in thickness d has been decreased with a factor of two, the residue S_N has been decreased by a factor of ten as compared to the results obtained with relative ARXPS measurements.

5.3. Correction on relative ARXPS measurements

With the results of absolute ARXPS measurements, we again can fit eq. (15), now with only one parameter: the constant C. We performed a fit at a thickness d of 0.88, 0.93 and $0.98\lambda_{SiO_2}$ respectively and tabulated the results in table 1, from which we may conclude:

$$C = 3.6 \pm 0.3\ (\pm 8\%).$$

Also the values of the residue S_R are given in table 1. The result is shown in fig. 6, where the theoretical curve is shown as a dotted line and the thickness d and constant C equal $0.93\lambda_{SiO_2}$ and 3.6, respectively. With this correction, we have decreased the error in constant C with a factor of four when compared to

Table 1
Correction on relative ARXPS measurements

Thickness d of oxide layer (λ_{SiO_2})	Constant C	Residue S_R
0.88	3.3	6×10^{-3}
0.93	3.6	8×10^{-3}
0.98	3.9	1×10^{-2}

The constant C, as given in eq. (15), has been fitted, using the thickness d, found with absolute ARXPS measurements.

relative ARXPS measurements. From table 1, we see that the residue S_R has not changed significantly (now in this correction we have only one parameter: the constant C), so we may conclude that the large errors in fitting eq. (15) are due to a strong correlation between the two parameters. This can also be seen in fig. 6 where the two theoretical curves are shown for different sets of optimal values of thickness d and constant C: relative ARXPS measurements and the correction on relative ARXPS measurements, respectively. The residue S_R is not strongly affected by a change in the parameters.

For the thickness d of a native oxide layer on silicon we found $0.93 \pm 0.05\lambda_{SiO_2}$ ($\pm 5\%$). The IMFP values for the photoelectrons in the silicon substrate and native oxide layer can be taken from the literature [13], where they equal 27.9 and 28.8 Å, respectively. With these values we find a thickness of the native oxide layer on silicon of 27 ± 1 Å ($\pm 5\%$), a value that agrees well with the literature [11,28]. For the constant C in eq. (15) we found a value of 3.6 ± 0.3 ($\pm 8\%$). With the IMFP of silicon and silica taken from the literature [13], we can estimate the atomic concentration ratio of silicon in the substrate to that in the native oxide layer to be 3.7 ± 0.3 ($\pm 8\%$).

We performed ARXPS measurements at photoelectron take-off angles above 70°, but, as already stated in section 2, the effect of aperture on the photoelectron energy distribution may not be neglected in this region and therefore these measurements were not used in the calculations.

6. Discussion

In the literature, eq. (1) is commonly used for the interpretation of ARXPS measurements and the calculation of layer thicknesses [1–5,9–11]. In this report we show which conditions the spectrometer has to fulfil to permit utilization of this equation, neglecting the effect of the electron energy analyser acceptance angle or the aperture on the photoelectron energy distribution.

Obtaining quantitative information from ARXPS measurements is an elaborate task and one must be cautious in interpreting these results. In film thickness measurements by relative ARXPS experiments, two parameters must be determined. As we showed in the case of a native oxide layer on silicon, errors in these parameters are large due to a strong correlation between these two parameters. Absolute measurements enable us to eliminate one parameter: the constant C, and therefore the remaining parameter d can be determined with higher accuracy. These results of absolute ARXPS measurements then can be used to correct the relative ARXPS measurements, decreasing the error in constant C.

With absolute and relative ARXPS film thickness measurements in combination with a modified Levenberg–Marquardt method, we succeeded not only in giving confidence limits of the parameters, but also in reducing errors in these parameters, giving reliable quantitative results.

As we showed in section 2, with an aperture of 9°, its effect on the photoelectron energy distribution may be neglected at photoelectron take-off angles lower than 70°. In fig. 6 we see that relative ARXPS measurements begin to deviate strongly from the theoretical curve at photoelectron take-off angles above 70°. This effect was also seen by Yan et al. [11], but these authors fully ascribe this effect to surface roughness of the sample only. Yan et al. used relative ARXPS measurements for the determination of the oxide layer thicknesses and therefore errors due to correlation between the parameters in the theoretical curves must be accounted for. Secondly, their conclusion is based on measurements in the region where the effect of aperture may not be neglected as we have shown in this paper. Their conclusion that deviation of these measurements from the theoretical curves is only due to surface roughness must be revised.

7. Conclusions

In this report, we find that (i) the experimental set-up and sample have to fulfil certain conditions to permit utilization of ARXPS. One of the conditions is that with an aperture of 3° or 9°, the photoelectron

take-off angle should not exceed 80° or 70°, respectively, as compared to normal take-off angle. At larger photoelectron take-off angles, the effect of the aperture on the photoelectron energy distribution may no longer be neglected. (ii) Absolute ARXPS film thickness measurements are superior to relative ARXPS film thickness measurements. (iii) Errors in the film thickness measurements by means of relative ARXPS measurements cannot be avoided. The two parameters, the thickness d and constant C, in the commonly used eq. (15) strongly correlate. (iv) The native oxide layer on silicon is 27 ± 1 ($\pm 5\%$) Å thick and the ratio of the silicon atom concentration in the substrate to that in the native oxide layer is 3.7 ± 0.3 ($\pm 8\%$). (v) The combination of absolute and relative ARXPS film thickness measurements and a LM fit procedure is well suited for the study of thin layers and gives reliable quantitative results.

References

[1] C.S. Fadley, R.J. Baird, W. Siekhaus, T. Novakov and S.Å.L. Bergström, J. Electron Spectrosc. 4 (1974) 93.
[2] C.S. Fadley, J. Electron Spectrosc. 5 (1974) 725.
[3] C.S. Fadley, Prog. Surf. Sci. 16 (1984) 275.
[4] Y.M. Cross and J. Dewing, Surf. Interf. Anal. 1 (1979) 26.
[5] H. Ebel, M.F. Ebel and E. Hilbrand, J. Electron Spectrosc. 2 (1973) 277.
[6] L.B. Hazell, I.S. Brown and F. Freisinger, Surf. Interf. Anal. 8 (1986) 25.
[7] T.D. Bussing, P.H. Holloway, Y.X. Wang, J.F. Moulder and J.S. Hammond, J. Vac. Sci. Technol. B 6 (1988) 1514.
[8] T.D. Bussing and P.H. Holloway, J. Vac. Sci. Technol. A 3 (1985) 1973.
[9] J. Halbritter, J. Mater. Res. 3 (1988) 506.
[10] C. Battistoni, G. Mattogno and E. Paparazzo, Surf. Interf. Anal. 7 (1985) 117.
[11] Y.L. Yan, M.A. Helfand and C.R. Clayton, Appl. Surf. Sci. 37 (1989) 395.
[12] M.P. Seah and W. Dench, Surf. Interf. Anal. 1 (1979) 2.
[13] J.C. Ashley and C.J. Tung, Surf. Interf. Anal. 4 (1982) 52.
[14] S. Tougaard, J. Vac. Sci. Technol. A 5 (1987) 1230.
[15] S. Tougaard and P. Sigmund, Phys. Rev. B 25 (1982) 4452.
[16] B.C. Henke, Phys. Rev. B 6 (1972) 94.
[17] J.H. Scofield, J. Electron Spectrosc. 8 (1976) 129.
[18] F.O. Ellison, J. Chem. Phys. 61 (1974) 507.
[19] R.F. Reilman, A. Msezane and S.T. Manson, J. Electron Spectrosc. 8 (1976) 389.
[20] R. Fletcher, A. Modified Marquardt Subroutine for Non-Linear Least-Squares Fitting, UK Atomic Energy Authority Research Group, Theoretical Physics Division, AERE-R. 6799, Harwell, Berkshire, 1971.
[21] S.Y. Kim and K. Vedam, Appl. Opt. 25 (1986) 2013.
[22] Kratos Xsam 800 Operators handbook.
[23] D. Briggs and M.P. Seah, Practical Surface Analysis by Auger and X-ray Photoelectron Spectroscopy (Wiley, Chichester, 1983) p. 431.
[24] Manual DS800.
[25] D.A. Shirley, Phys. Rev. B 5 (1972) 4709.
[26] M. Nakazawa, S. Kawase and H. Sekiyama, J. Appl. Phys. 65 (1989) 4014.
[27] M. Nakazawa, Y. Nishioka, H. Sekiyama and S. Kawase, J. Appl. Phys. 65 (1989) 4019.
[28] H. Ibach, H.D. Bruchmann and H. Wagner, Appl. Phys. A 29 (1982) 113.